



HAL
open science

Finite element simulation of a steel cable-rubber composite under bending loading: influence of rubber penetration on the stress distribution in wires

Matthieu Bonneric, Véronique Aubin, Damien Durville

► To cite this version:

Matthieu Bonneric, Véronique Aubin, Damien Durville. Finite element simulation of a steel cable-rubber composite under bending loading: influence of rubber penetration on the stress distribution in wires. *International Journal of Solids and Structures*, In press, 10.1016/j.ijsolstr.2018.10.023 . hal-01904549

HAL Id: hal-01904549

<https://centralesupelec.hal.science/hal-01904549v1>

Submitted on 25 Oct 2018

HAL is a multi-disciplinary open access archive for the deposit and dissemination of scientific research documents, whether they are published or not. The documents may come from teaching and research institutions in France or abroad, or from public or private research centers.

L'archive ouverte pluridisciplinaire **HAL**, est destinée au dépôt et à la diffusion de documents scientifiques de niveau recherche, publiés ou non, émanant des établissements d'enseignement et de recherche français ou étrangers, des laboratoires publics ou privés.

Finite element simulation of a steel cable - rubber composite under bending loading: influence of rubber penetration on the stress distribution in wires

Matthieu Bonneric^{a,*}, Véronique Aubin^a, Damien Durville^a

^a*MSSMat Laboratory, CentraleSupélec, CNRS UMR8579, Université Paris-Saclay*

Abstract

Fatigue design of cables requires to assess the stresses of individual wires during in-service loadings. Specific applications need steel cables to be embedded in a rubber matrix. In such cases, the adhesive bonding between wires and matrix might impact the stress distribution in wires. This paper presents a finite element model of cable coated with a rubber matrix subjected to a bending loading. Wires are represented with a strain beam model taking into account for non linear phenomena, such as contact friction between wires and elastoplastic behavior. A 3D model for the matrix surrounding the cable is coupled with the beam model. The impact of matrix penetration inside the cable is also studied. This work proposes a multi-scale approach to account for local interactions between infiltrated matrix and wires under bending loading in the coated cable model. The behavior of infiltrated matrix subjected to a shearing loading induced by longitudinal inter-wire displacements is investigated using both analytical calculations and local FE simulations with ABAQUS software. Based on the results at

*MSSMat Laboratory, CentraleSupélec, CNRS UMR8579, Université Paris-Saclay
Email address: matthieu.bonneric@centralesupelec.fr (Matthieu Bonneric)

the microscopic scale, “junction” elements are introduced in the coated cable model to account for matrix penetration, by coupling neighbor wires’ displacements. The model is compared with experimental measurements of cables slightly and fully penetrated by matrix. The influence of matrix penetration on the stress distribution is eventually discussed. It is found that the limitation of inter-wire motions due infiltrated matrix induces tensions in wires, which are responsible for increases of the bending stiffness and of the maximum stresses in wires.

Keywords:

cable simulation, bending loading, steel cord - rubber composite, rubber penetration, multiscale approach

1. Introduction

Steel cables are commonly used in various fields, as parts of complex structures (pneumatic tire reinforcements, bridge suspensions, etc...). In order to guarantee a safe design of these structures, one needs to predict the mechanical behavior of cable under in-service loadings. Failure being due to damage localization within the individual wires, the local state of stress of wires has to be known. As well, cable design may be improved by the understanding of wire kinematics. To address these issues, finite element simulation of cable is a useful tool providing rich information.

Several authors worked on the accurate prediction of cable behavior and built models accounting for non-linear phenomena such as elastoplastic behavior or contact friction. Jiang *et al* proposed a concise finite element model taking advantage of the helical symmetry of a 7-wire cable for an axial ten-

sion loading, in order to study contact stresses between wires [1]. Judge *et al* studied the development of high local contact stresses and local yielding for both 7-wire and 120-wire spiral cables subjected to an axial loading [2]. Wang *et al* modelled a 7x19 wire cable loaded with cyclic tension-tension in order to assess fretting wear evolution of steel wires [3]. Kmet *et al* investigated the behavior of a 61-wire cable bent over a saddle subjected to axial tension [4]. They studied the influence of axial loading and saddle radius on the resultant stress in different cable sections of the bent area. The results were validated against strain gauge measurements assuming linear elastic behavior of wires.

Some works specially deal with the cable behavior under a bending loading. Nawrocki and Labrosse studied the wire motions in a 7-wire cable [5]. They found inter-wire sliding to be predominant in bending. Jiang studied a 7-wire cable under a pure bending loading [6]. They noted that every wire bends independently, and is consequently subjected to a pure bending. Besides, contact friction is found to have very little influence on global behavior of cable and on inter-wire sliding, since contact pressures are negligibly small. Zhang *et al* found similar results a few years later [7]. They were interested in the mechanisms governing the bending stiffness of a 7-wire cable, and specially studied the influence of the lay angle, inter-wire motions, pre-tension and contact friction.

Several studies [2, 8, 9] compared their results with both analytical models such as Costello's one [10], and experimental axial loads measurements from Utting's work [11]. This comparison highlighted the importance of considering elastoplastic behavior of wires and contact friction to get an ac-

curate description of the mechanical state of cable. It is worth noting that macroscopic responses of cable are sensitive to such local phenomena, and are suitable for the validation of numerical models.

For some applications, cables may be embedded in a rubber coat. In such cases, wires stick to the rubber matrix they are in contact with. One may ask what is the impact of the adhesive bonding between wires and matrix on the stress distribution of wires, and how the infiltration of the matrix inside the cable might affect this distribution. **To the best knowledge of the authors**, there is no previous study using cable simulation to answer this question. Indeed, in such cases composite plies models are usually used instead of cable models [12–14], and local stresses of wires are not assessed since cables are described as simple cylinders with elastic anisotropic properties. **As a consequence, these models cannot capture the full complexity of the interactions between cable and matrix, which involve several scales from the local mechanical loading applied to the matrix between wires up to the cable level. In order to tackle this issue, this work proposes a multi-scale approach allowing to account for wire-matrix interactions in a coated cable model, while preserving a reasonable computational cost by coupling beam models for wires with a 3D model for matrix.**

In this framework, the objective of the present study is to investigate the influence of the rubber matrix on the behavior of a coated cable, for the case of a bending loading. Section 2 describes a model of a cable coupled with rubber matrix, for which no matrix is infiltrated inside the cable. A cable - rubber composite subjected to a bending loading is simulated then, and

experimental measurements are used to validate the model. In section 3, an approach is proposed to account for matrix penetration, inspired by the analysis of wire kinematics from previous simulation. Two methods are proposed in order to identify parameters for this model, based on analytical calculations and local simulations of the interactions between wires and rubber matrix respectively. In section 4, a coated cable fully infiltrated and subjected to a bending loading is simulated. The role of rubber matrix is discussed in section 5.

2. FE model of steel cable - rubber composite

2.1. Modelling of steel cable

In this work cable simulations are performed with Multifil code, which is dedicated to the simulation of entangled materials and uses a kinematically enriched strain beam model with 9 degrees of freedom to model wires. The use of proximity zones to define contact areas enables to account for contact friction between wires while preserving an efficient computation cost. Complete descriptions of both beam kinematic and contact friction definition are given elsewhere [15], as well as some applications of Multifil code [16, 17]. Wires are meshed with quadratic elements, and boundary conditions are imposed either by defining the movement of cable ends or by using rigid bodies.

The elastoplastic behavior of wires is also considered. As the main concern of this study is the bending loading for which axial stress is predominant, it was only developed an uniaxial model in a first approach. The plasticity

criterion expressed in Eq. 1 is applied to the axial stress σ :

$$|\sigma - X| - \sigma_0 \leq 0 \quad (1)$$

where σ_0 is the initial yield stress, and X a non-linear kinematic hardening from Armstrong and Frederic model [18], obeying the following equation:

$$\dot{X} = C\dot{\varepsilon}_p - \gamma X\dot{p} \quad (2)$$

In this expression, C and γ are material parameters, ε_p is the plastic strain, and p is the cumulative plastic strain defined by $p(t) = \int_0^t |\dot{\varepsilon}_p(s)| ds$.

2.2. Introduction of a rubber matrix

To account for the rubber matrix surrounding the cable, a 3D mesh of linear elements is used. It is obtained by extruding a radial mesh along cable direction, as shown in figure 1a. As it can be observed in figure 1b, the mesh is coarse compared to the wire diameter, and matrix elements overlap the wires of the outer layer of the cable.

Junction elements are generated in the overlapping regions to account for the adhesive bonding between matrix and wires. Each of these elements couples the displacements of a pair of material particles ξ_w and ξ_r from a same cable section belonging to wire and rubber respectively, whose positions are described with vectors \mathbf{x}_w and \mathbf{x}_r . This coupling is achieved by means of an elastic spring of stiffness k : two opposite forces are applied on both particles, whose magnitude F is given by:

$$F = k \|\mathbf{x}_w - \mathbf{x}_r\| \quad (3)$$

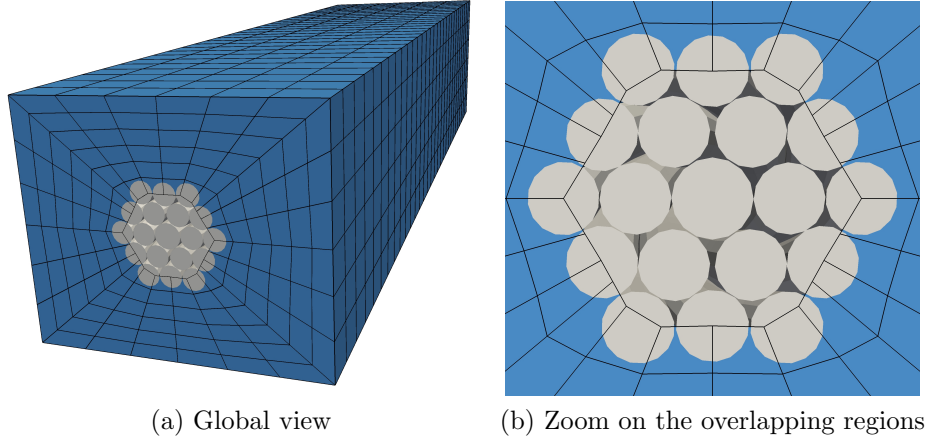


Figure 1: View of the mesh of the matrix

Junction elements are created for every finite element node of wire inside the matrix. Thus, a matrix element may be tied to several wire nodes, depending on the mesh sizes of wires and matrix. Besides, let's remind that wire kinematic is richer than matrix's one. With this in mind, the use of junction elements can simply be seen as a penalty method chosen to enforce the coupling between wires and matrix while avoiding motion incompatibilities.

Matrix constitutive behavior is described with an isotropic elastic law. The use of such constitutive equations instead of an hyperelastic law, commonly used for rubbers, is justified in section 2.4.

2.3. *Experimental measures and boundary conditions*

An experimental device was developed to compare simulation results with experimental measurements. It is made of two plates between which a steel cable - rubber composite specimen is bent (figure 2). The loading is defined

by the distance d between the plates, which is gradually reduced by moving one plate in translation while the other remains still. This distance is controlled with a position sensor. The radius R of the quasi-circle formed by the median fiber of the bent specimen can then be calculated using the expression:

$$R = \frac{1}{2}(d - t) \quad (4)$$

where t is the specimen thickness. In the following developments this parameter will be used to describe the bending loading. Besides, the reaction force applied to the plates is also measured to quantify the response of the bent specimen.

Similar boundary conditions will be applied in the simulations, using two rigid planes (figure 3). It should be noted that for a significant bending ($R < 10$ mm), which will be mainly examined in what follows, the ends of the

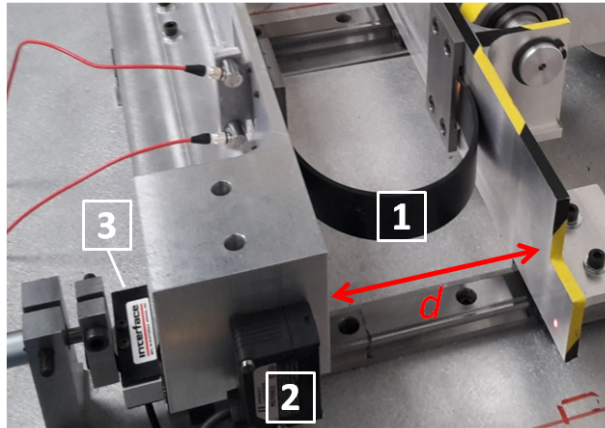


Figure 2: Experimental device to bend composite rubber - steel cable specimens : 1. Specimen - 2. Position sensor - 3. Load Cell

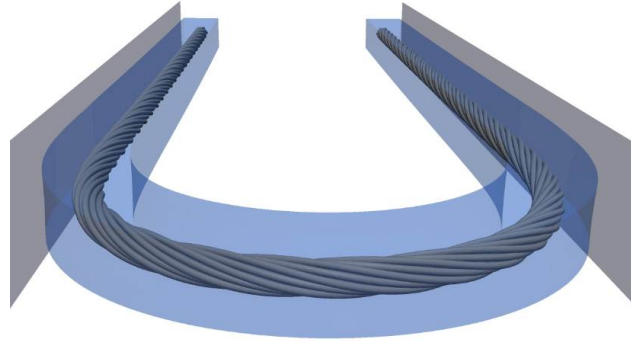


Figure 3: Bending of a composite specimen with Multifil

specimen are far from the bent area. Indeed, the specimen length is then ten times longer than the bent portion, which is in the middle of the specimen. In such case, it is assumed that the force applied on the experimental device to clamp the specimens has no influence on the measured force. Therefore, the clamping force is not accounted for in the modelling of the bent specimen.

2.4. Simulation of a rubber specimen

It is intended to validate the modelling of the composite specimen by using the prediction of the reaction force. In a first place, the contribution of rubber to this quantity was validated, and the associated error was quantified. To do so, simulations have been carried out on full rubber specimens using different constitutive equations, and compared with experimental measurements.

A full rubber specimen of width $w = 20$ mm and thickness $t = 3.2$ mm has been tested on the experimental device. These dimensions are associated to a measure uncertainty of 0.1 mm. ABAQUS/Standard was used instead

of Multifil for the simulations, in order to evaluate both isotropic elastic and hyperelastic behaviors. The elastic law is parameterized by a Young modulus $E = 5.5 \text{ MPa}$, whose value is estimated from tensile test and coincides with the secant modulus measured at 20% strain. The Poisson's ratio is set to $\nu = 0.495$ to account for rubber incompressibility. The hyperelastic behavior is represented using the ABAQUS Marlow model [19], which is a first invariant constitutive model as described in [20]. It is directly identified by ABAQUS software from tensile test data. Due to a lack of data, material's viscous behavior was not considered. Linear C3D8H elements were used for the simulation, whose dimensions are between 0.3 and 1 mm.

Figure 4 plots the magnitude of the reaction force versus the radius R . Calculations have been performed for several thickness's in order to evaluate the impact of measure uncertainty on the reaction force. It is to be noted

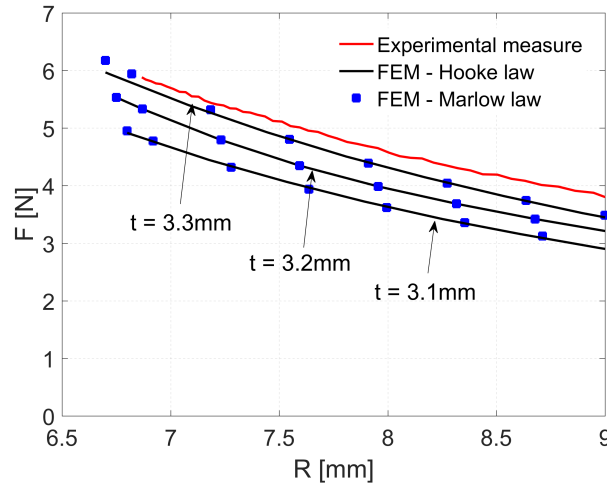


Figure 4: Reaction force of full rubber specimens under bending loading

that due to the measurement range of the position sensor, experimental data only provide information about the last millimeters of the loading.

It can be observed that the use of an elastic law leads to the same reaction force than the use of the hyperelastic one's. This result is consistent with rubber response, whose true strain values do not exceed 30 %. It is observed that numerical forces are 10.5 % on average lower than experimental measurements though. These differences can be explained by the errors due to both the measure uncertainty of the thickness, and the non consideration of the material's viscous behavior.

For cable - rubber composite simulations, **one** will seek to limit this error by reducing the contribution of rubber to the reaction force. To do so, thin specimens of thickness $t = 2.4 \pm 0.1$ mm will be used for both experiments and calculations.

It is preferred to have specimens of significant width to carry out the experiments. In this study, **specimens of width 10 mm are used**, allowing the enforcement of accurate boundary conditions by preventing any undesired rotation of the specimen. At least 5 cables are then required to counterbalance the contribution of rubber to the reaction force.

However, the composite simulation considers only one cable, and doesn't allow the enforcement of periodic boundary conditions on the lateral sides of the specimen. To be consistent with numerical results, measured loads are thus divided by the number N of cables contained in the real specimens. Also, the width of numerical specimens is defined by $w_0 = w/N$ with w the

width of the real specimen, meaning $w_0 = 2$ mm. By doing so, it is implicitly assumed that the ratio F/w doesn't depend on the specimen width. However, the non consideration of periodic boundary conditions on the lateral sides of rubber questions the validity of this hypothesis. Two simulations of a full rubber specimen of thickness 2.4 mm have been performed in order to quantify the associated error, considering the two widths from real specimen and numerical specimen respectively. It is then observed a 9.2% decrease of the ratio F/w at $R = 7$ mm by reducing the width from 10 mm to 2 mm.

In the next sections, cable - rubber composite simulations will be performed on specimens having thickness and width of 2.4 mm and 2 mm respectively. The elastic law and its parameterization presented in this section will be used to account for the rubber surrounding the cable, since the use of elastic and hyperelastic laws lead to the same global response. Besides, full rubber simulations can be used to evaluate the rubber contribution to the reaction force of such composite specimens, assuming that the global response of rubber remains the same with or without cable. This contribution is found to be 0.2 N. Based on the previous analysis, the error associated to the contribution of rubber to the reaction force in the composite model is 0.04 N (constitutive equations and reduction of rubber width), which is a negligibly small value.

2.5. Simulation of a composite specimen

The 19-wire cable shown in figure 5 has been considered in order to test the composite model. It is made of two layers #2 and #3 of helical wires of 175 μ m diameter (Wire 1) winded with a pitch length of 10 mm around

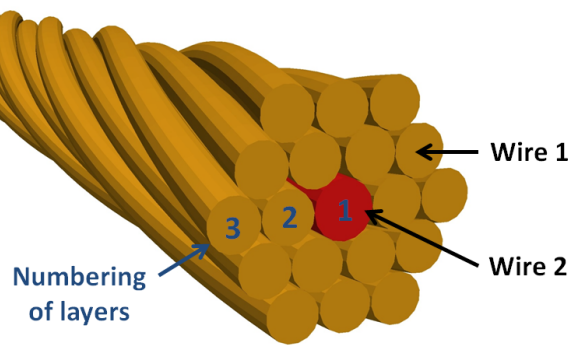


Figure 5: 19-wire cable of length 10 mm

a straight wire of 200 μm diameter (Wire 2) in layer 1. All the wires are meshed with a beam assumption using elements of length 0.33 mm.

The material parameters used to describe wires behavior were identified from monotonic tensile tests and are given in table 1.

The coefficient of the Coulomb's law used to describe friction between wires was set to 0, after testing values 0 and 0.3. It has been verified that this parameter has no influence on both the stress distribution and the reaction force for the present loading. This result can be explained by the absence of tension in the cable which drastically reduces the magnitude of frictional contact interactions between wires, in accordance with previous research [1,

Table 1: Material properties of wires

		Wire 1	Wire 2
Elastic properties	E [GPa]	193	201
	ν [-]	0.3	0.3
Plastic properties	σ_0 [MPa]	2161.6	2010
	C [MPa]	853394	433196
	γ [-]	997	575

7]. Following to the previous section, **one considers** a specimen having width and thickness of 2 mm and 2.4 mm respectively, and of length 100 mm. The dimensions of the rubber mesh are between 0.2 and 0.6 mm. Such a specimen leads to a total of 160,500 degrees of freedom (including both wires and rubber). The simulation of its bending is then carried out in 66 increments using an implicit scheme.

Experimental measures on the bending test were carried out on two composites A and B. Both of them are made of the same 19-wire cable and of the same rubber. The only difference between them is the penetration rate of the matrix inside the cable: composite A isn't infiltrated whereas composite B is fully penetrated, as shown in figure 6.

Figure 7 plots the reaction force F as a function of radius R , for both experiments and simulation. It is to be noted that simulation is in very good agreement with the experimental measurements made on the non infiltrated composite, which demonstrates the ability of the model to predict cable response for the case where no rubber penetrates the cable.

It can also be observed that composite B is stiffer than composite A for

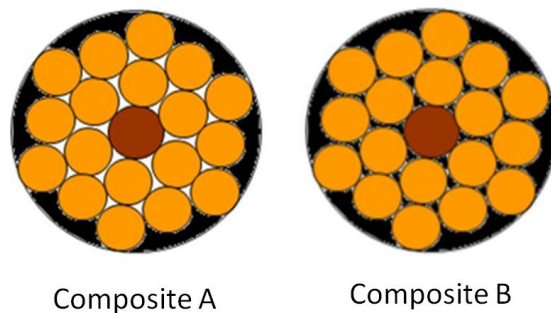


Figure 6: Schematic representation of composites A and B

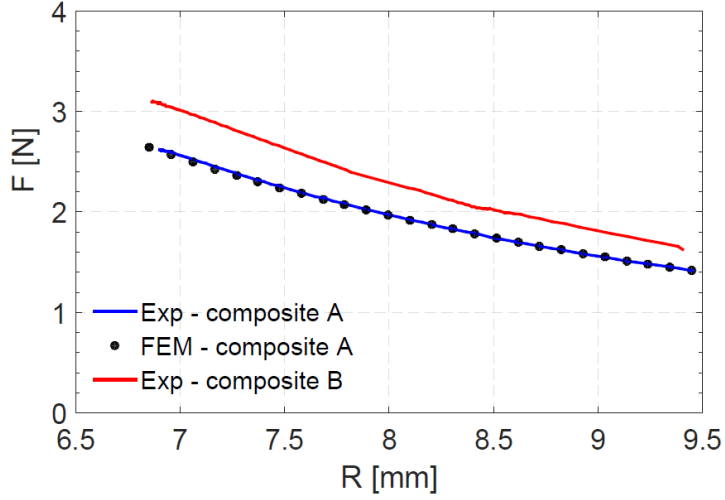


Figure 7: Comparison of the reaction force from composite simulation to experimental measurements

high curvatures: when $R = 6.75$ mm, the reaction force of composite B is 18% more important than the one of composite A. One may assume that this stiffening comes from local interactions between neighbor wires, due to the bond exerted by the infiltrated matrix.

In order to understand the nature of these interactions, the relative motions of neighbor wires were investigated in the simulation without infiltrated matrix. The displacement vector \mathbf{u} of any material particle of wire can be decomposed into $u_L \mathbf{e} + \mathbf{u}_T$ to discriminate longitudinal and transverse motions, \mathbf{e} being the unit tangent vector to the wire. Relative displacements $\Delta \mathbf{u}$ between the centers of neighbor wires were then computed. The comparison of the two components Δu_L and Δu_T reveals that longitudinal component is predominant. This is illustrated on figure 8, which plots both Δu_L and Δu_T for a couple of neighbor wires, as a function of the curvilinear abscissa s of the bent cable. Δu_L can reach a value of 50 μm . Besides, it should be noted

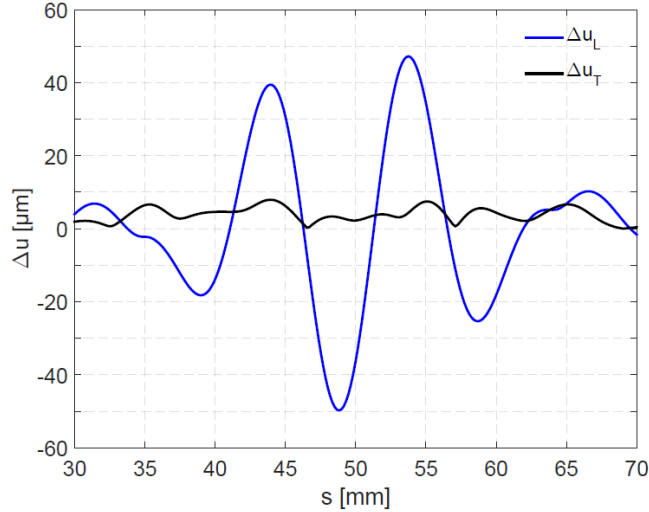


Figure 8: Relative displacement between 2 neighbor wires from layers 1 and 2 as a function of curvilinear abscissa - $R = 7$ mm

that the presence of rubber outside of the cable limits radial relative displacements and that the bent cable remains compact. The transverse component Δu_T derives from the rotation of wires around their neighbors, whose angle doesn't exceed 3° . These results are consistent with previous works [5], and confirm that the mechanical response of the cable is governed by longitudinal inter-wire motions when subjected to a bending loading.

Thus, it seems reasonable to think that the local interactions between neighbor wires and infiltrated matrix are mainly induced by inter-wire longitudinal displacements.

The introduction of a 3D mesh of rubber inside the cable is not convenient considering the different scales involved. Indeed, rubber thickness can reach values of about $1 \mu\text{m}$ between wires, whereas specimens's section is millimeter's sized. Building a 3D mesh would introduce strong size gradient as well

as a lot of degrees of freedom, meaning high computation cost. The following section proposes a different approach to account for infiltrated matrix, based on the study of local interactions between matrix and neighbor wires.

3. Local interactions between wires and matrix

3.1. Infiltrated matrix modelling

Considering the previous analysis of inter-wire motions, it can be assumed that the main impact of the infiltrated matrix is the limitation of longitudinal motions between neighbor wires. The latter can also be considered as a coupling of wire displacements. It is then proposed to use junction elements, described in 2.2, to account for local interactions between wires and matrix.

M planes $\{P_1, P_2, \dots, P_M\}$, normal to cable axis and equally spaced, are used to generate a set of M junction elements for each pair of neighbor wires. The junction element $J_N^{(I,J)}$ couples a pair of material particles ξ_N^I and ξ_N^J , belonging to two wires I and J respectively. In the initial configuration, the positions $\mathbf{x}_N^I(0)$ and $\mathbf{x}_N^J(0)$ of these particles are defined by the intersection of the considered wires with the normal plane P_N .

For a given moment t , the junction element $J_N^{(I,J)}$ is responsible for two opposite forces applied on particles ξ_N^I and ξ_N^J , whose magnitude F is proportional to the longitudinal component of the relative displacement of the two particles :

$$F(t) = K \left\| dx_N^{(I,J)}(t) - dx_N^{(I,J)}(0) \right\| \quad (5)$$

with

$$dx_N^{(I,J)} = \left\langle \mathbf{x}_N^J - \mathbf{x}_N^I, \mathbf{e}_N^{(I,J)} \right\rangle \quad (6)$$

In the latter expression, $\mathbf{e}_N^{(I,J)}$ is the mean of the tangent vectors of wires I and J at the respective positions \mathbf{x}_N^I and \mathbf{x}_N^J .

With the present approach, the local interactions between wires and matrix are described with the stiffness K . Two methods were then developed to evaluate this stiffness. The first one is based on an analytical evaluation of the resultant load applied to wires by the deformed matrix. This method provides a better understanding of the influential parameters, but requires the assumption of a linear elastic behavior within small strain framework. The second method consists in direct FE simulations of the matrix shearing in order to get accurate evaluations of the stiffness.

The analytical evaluation of the reaction force is first described. Let's suppose that the rubber between two wires is only subjected to the shearing loading induced by the longitudinal relative displacement Δu_L between two neighbor wires. Furthermore, linear elastic behavior of the matrix as well as small strains framework are assumed. The shear stress τ of an elementary volume of rubber of thickness d can therefore be expressed as $\tau = \mu \Delta u_L d$, where $\mu = E/(1 + \nu)$ is the shear modulus.

Using the parameterization given in figure 9, the magnitude of the resultant load applied by the sheared matrix to a portion of wire of length l is calculated with the following formula :

$$F = \int_{-\pi/2}^{\pi/2} \mu \frac{\Delta u_L}{d(\theta)} R d\theta l \quad (7)$$

leading to :

$$F = \int_{-\pi/2}^{\pi/2} \mu \frac{\Delta u_L}{d_m + 2R(1 - \cos(\theta))} R d\theta l \quad (8)$$

The comparison of Eq. 5 and Eq. 8 leads to the following expression for the stiffness K :

$$K = \int_{-\pi/2}^{\pi/2} \frac{\mu}{d_m + 2R(1 - \cos(\theta))} R d\theta L_0 \quad (9)$$

where L_0 is the distance between two junction elements.

This analytical formulation exhibits that matrix response not only depends on rubber constitutive behavior, but also on the minimum distance between neighbor wires d_m .

However, the significant inter-wire motions resulting from the bending of

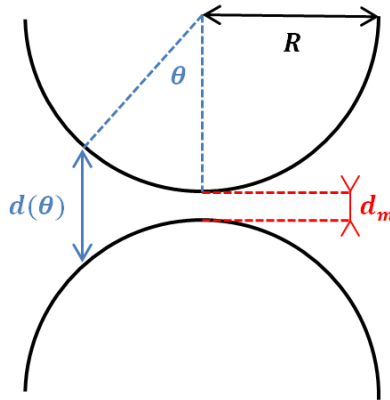


Figure 9: Parameterization of the geometry between two wires

the composite specimen are responsible for large strain in the matrix. One may question the validity of the strong assumptions made to evaluate K , which are linear elastic behavior and the use of small strains framework. This is why local FE simulations of the infiltrated matrix sheared by wire longitudinal motions have also been performed, in order to get a more precise method of evaluation of K and to compare the results from both approaches.

3.2. Local FE simulations of matrix shearing

In order to evaluate the response of the infiltrated matrix subjected to the longitudinal displacements between two neighbor wires, let's consider a volume of rubber between two wires, of length $L_0 = 500 \mu\text{m}$ and such as $|\theta| \leq 55^\circ$ (figure 10). The impact of the minimum thickness d_m was also investigated, and several geometries were generated with $d_m \in [2 - 10] \mu\text{m}$, coinciding with the inter-wire minimum distances measured on real specimens.

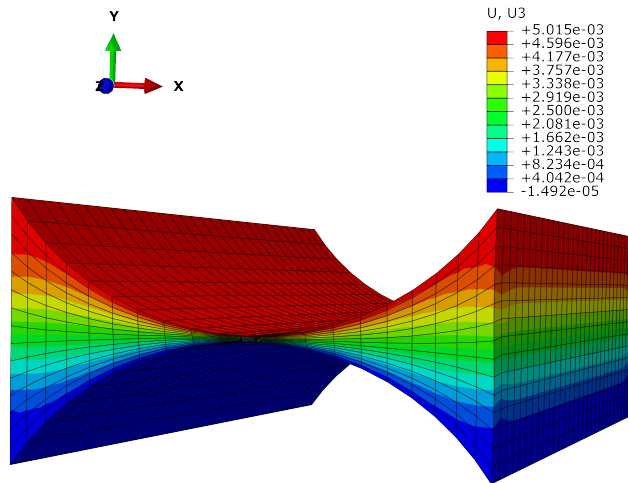


Figure 10: Shearing of the matrix between 2 wires

Simulations were then performed with ABAQUS/Standard. The Marlow model from ABAQUS software was used to account for the hyperelastic behavior of rubber. The wires were modelled with rigid bodies, since steel wires are much more stiffer than rubber. These rigid bodies were used to apply boundary conditions accounting for a longitudinal displacement of the upper wire. All the degrees of freedom of the lower rigid body were locked, whereas a translation Δu_L was applied to the upper one in the wire direction. The displacement value was set to $2.5 d_m$ in order to get a large strain. Rubber was meshed with 15 elements within its thickness using linear C3D8H elements.

Figure 11 plots the resultant load F applied by the rubber to the upper wire as a function of the imposed displacement. The response appears to be bilinear, with an increase of the slope of 80% shortly after the beginning

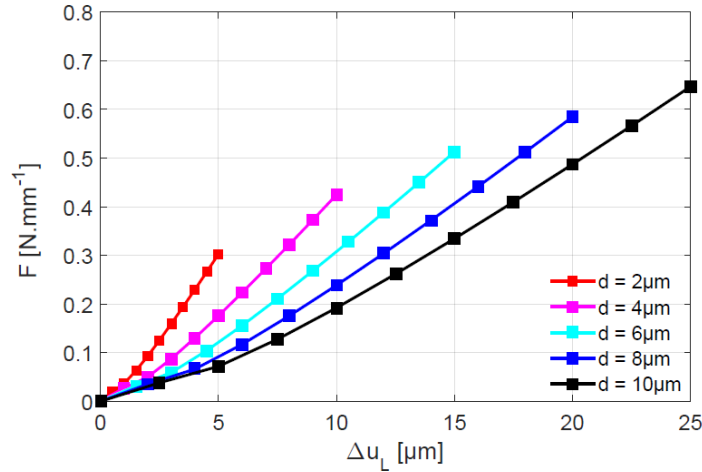


Figure 11: Resultant load applied by the matrix to moving wires - Influence of the minimum thickness

of loading. Non-linear effects due to large strains may explain this change of slope, which is not depicted by the analytical model. In particular, the experimental tensile curve used by ABAQUS to describe the hyperelastic behavior with Marlow model is not linear, and the nominal stress-strain curve exhibits an increase of slope of 30 % beyond 25 % strain.

Nevertheless, as the change of slope occurs at the very beginning of wire displacement, the assumption of a linear response is made, and stiffness's K such as $F = K\Delta u_L$ are evaluated for each minimum thickness d_m by mean of a linear regression.

These results confirm the sensitivity of the stiffness K to rubber thickness d_m .

The two methods of evaluation of the stiffness's K were eventually compared. To do so, stiffness's were evaluated using the analytical method, after adapting the integration limits in Eq. 9 in order to consider the same geometry with both methods. The elastic law employed for analytical evaluation was parameterized with $E = 5.5$ MPa, whose value was estimated from tensile test and coincides with the secant modulus measured at 20 % strain, in accordance with small strain hypothesis. Poisson's ratio was set to $\nu = 0.5$ in order to account for rubber incompressibility.

The elastic law employed for analytical evaluation was parameterized with $E = 5.5$ MPa, whose value was estimated from tensile test and coincides with the secant modulus measured at 20 % strain, in accordance with small strain hypothesis. Poisson's ratio was set to $\nu = 0.5$ in order to account for rubber incompressibility.

The comparison of the stiffness's obtained with analytical evaluations and FE simulations is given in figure 12. The two methods provide comparable values in spite of the different assumptions made for both cases, which gives some credit to the obtained stiffness's. In the following section, these stiffness's are then introduced in the composite model, in order to study the influence of infiltrated matrix on cable behavior.

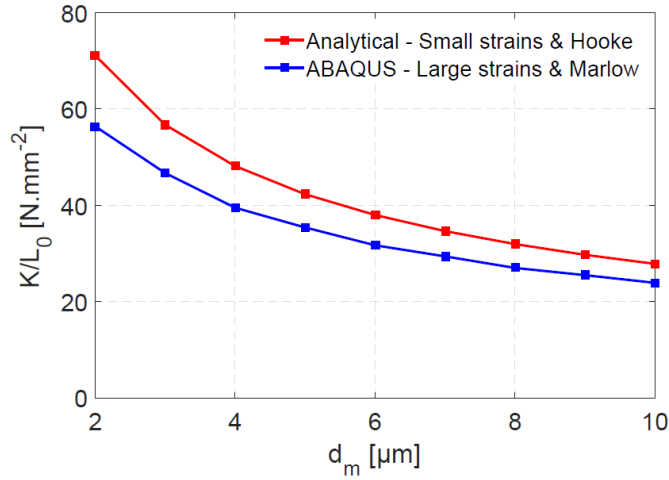


Figure 12: Evolution of the stiffness's K with matrix thickness d_m

4. FE simulations considering matrix infiltration

Simulations of an infiltrated specimen (composite B) were performed. The boundary conditions and parameterization described in 2.5 were imposed on the composite, and junctions elements between neighbor wires were introduced to account for infiltrated matrix. Elements stiffness's from both analytical calculation and simulation (figure 12) were tested.

Figure 13 plots the force applied to the bent specimen infiltrated by the matrix as a function of radius R , and compares the simulated results to experimental measurements. It is observed that simulated specimens are much more stiffer than the real one, the simulated reaction forces being overestimated by between 45 % and 60 %. This point is discussed in section 5.

Besides, the relative difference between the two methods of evaluation of stiffness's K is very little compared to the difference with experiments. Thus, analyzing both simulations would be redundant. In what follows, **only the simulation obtained with the stiffness's K evaluated with ABAQUS simulations will be used, in order to understand the impact of infiltrated matrix.** Nevertheless, **one** will keep in mind that this simulation is not fully representative of the real behavior, meaning that local interactions between wires are exacerbated and more significant than in a real composite.

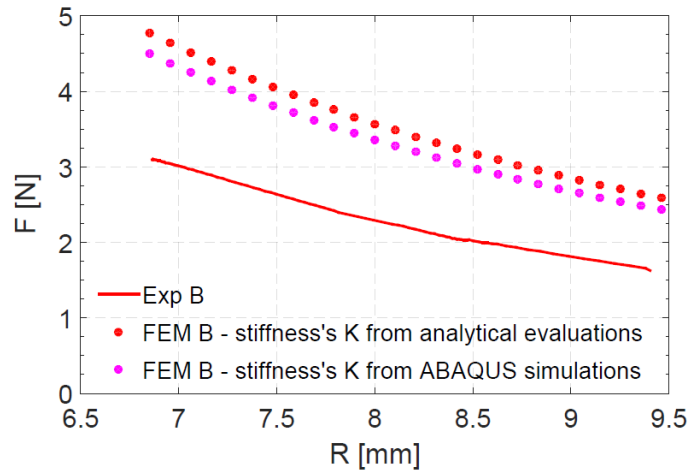


Figure 13: Comparison of the forces applied to the simulated infiltrated specimens with experimental measurements

Relative displacements between neighbor wires were considered, since junction elements' main function is to limit their longitudinal components. Figure 14 plots the relative displacements for a couple of neighbor wires as a function of the curvilinear abscissa of the cable, and compares the results for infiltrated and non infiltrated composites A and B. These displacements are computed at the centers of the wires. It is possible to note the effect of the junction elements, which induce a decrease of longitudinal inter-wire motions. Indeed, it is observed that the highest value of the longitudinal component is reduced by 20%. In the meantime, one can notice an increase of the transverse motions which allow to accommodate the loading. It should be reminded that these transverse motions are mainly due to rotations of wires around their neighbors, which are not limited by the junction elements. In reality, one would expect this transverse shearing of the matrix to be respon-

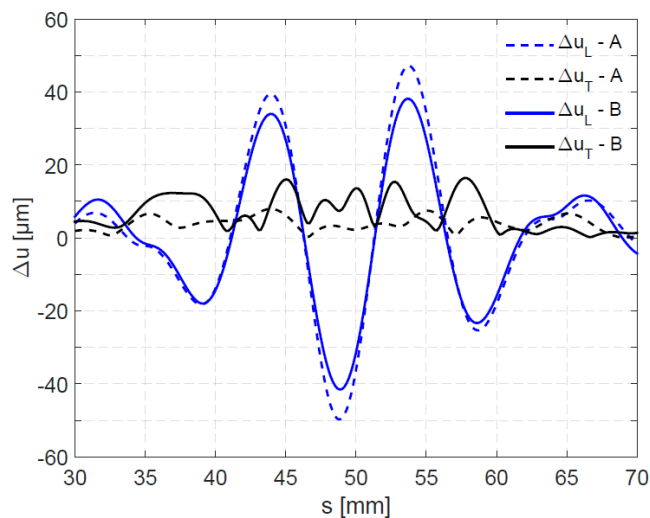


Figure 14: Evolution of the relative displacement between between 2 neighbor wires from layers 1 and 2 as a function of the curvilinear abscissa - Influence of infiltrated matrix - $R = 7$ mm

sible for an additional stiffening of cable, though far less significant than the one obtained by limiting longitudinal relative displacements.

These limitations are responsible for tensions in wires. This can be seen in figure 15, which exhibits a view of a cable section in the middle of the bent area for both composites A and B. In order to dispose of an appropriate scale to compare stresses from different wires and to facilitate interpretation, the value of the longitudinal stress in the wire centerline is attributed to the whole wire section. This results in a single color for each wire section on the viewing, which doesn't account for stress gradients in wire sections. For the case of non infiltrated composite A, the bending of each wire is independent from the bending of its neighbors. Consequently, wires are subjected to pure

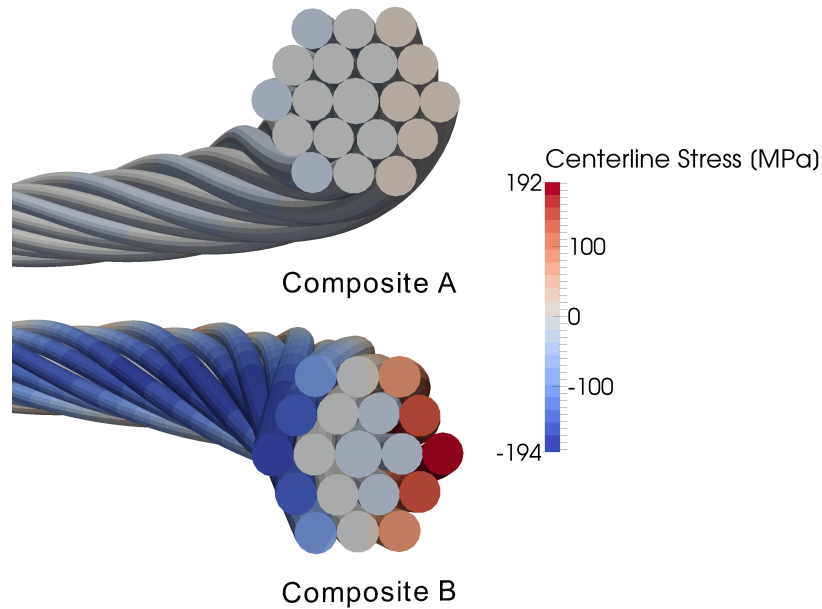


Figure 15: Comparison of the distribution of wire centerlines stresses within a section of bent cable - $R = 10$ mm

bending and the stress of wire centerlines is near-zero. To the opposite, the limitation of relative displacements between the neighbor wires of composite B leads to a different stress distribution. It can be observed a gradient of stress at the level of wire centerlines within the cable section, meaning that cable behavior approaches the behavior of an homogeneous beam.

The interactions between infiltrated matrix and wires are responsible for tensions in wires. In the following section, the impact of these tensions on the maximum stress distribution is discussed, in order to evaluate the potential harm from infiltrated matrix. Besides, the overestimation of the reaction force using the infiltrated composite model is discussed.

5. Discussion

5.1. Impact of matrix penetration on the maximum stress distribution

For the case of a bending loading, the study of cable durability requires to pay a particular attention to the stress distribution at the surface of wires. Indeed, these values coincide with the maximum stresses which are the most likely to provoke damage (fatigue crack initiation for instance). When considering the infiltrated specimen, the maximum stresses do not only depend on the evolution of stresses accross wires' cross sections, resulting from the bending of individual wires, but are also affected by the tensile stresses among wires induced by the infiltrated matrix. The impact of these tensile stresses on the maximum stress distribution at the surface of wires was investigated.

The infiltrated composite models previously described do not provide a

stress state representative of the real bent specimen, as indicated by the overestimation of the reaction force observed in 4. In order to get a more precise stress distribution for composite B, additional simulations have been performed, looking for a match between the simulated reaction force and the experimental measurements by varying the stiffness's values of the junction elements within a lower range. In a first approach, a unique value of the parameter K/L_0 was set for all the junction elements. A satisfying fit with experimental data has eventually been obtained by setting K/L_0 to 10 N.mm^{-1} , as it can be observed in figure 16. One can therefore assume that this simulation provides a more realistic stress distribution than the ones based on the junction elements' models presented in 3. Nevertheless, it should be kept in mind that since the stiffness of the junction elements does not depend on the distance between neighbor wires, the stress distribution does not strictly correspond to the real situation.

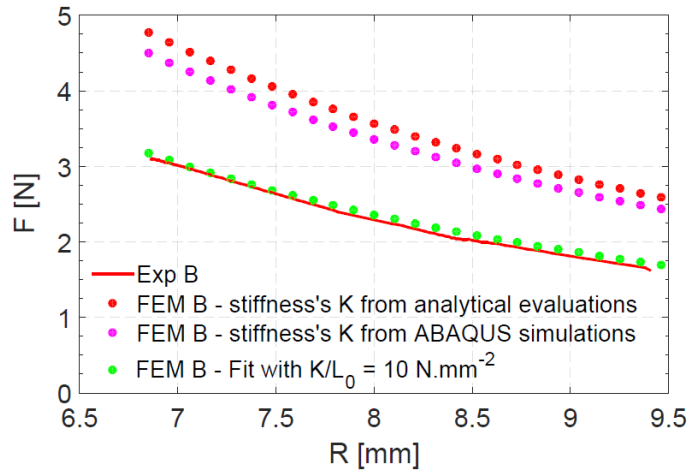


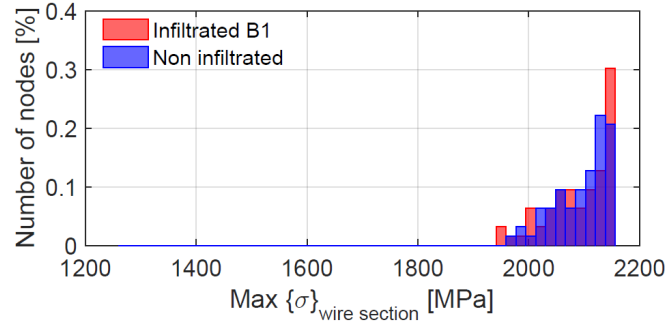
Figure 16: Fitting of the force derived by simulation of composite B with experimental measurements

In what follows, this last simulation is analyzed since it is the most representative of the real bent specimen. However, infiltrated composite simulation obtained in 4 with stiffness's identified from FE simulations of matrix shearing is still considered. By doing so, **it is intended** to have a better understanding, since the influence of infiltrated matrix on the maximum stress distribution is exacerbated. Thus, **one will discriminate composite B1 from composite B2**, referring respectively to the simulation presented in 4 and to the simulation fitting experimental data.

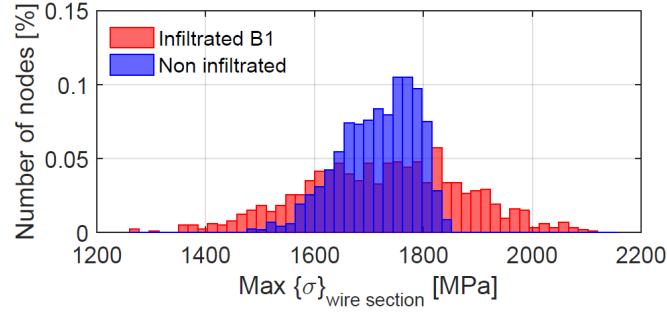
Figure 17 plots the maximum stress distribution associated to composite B1 for $R = 10$ mm, obtained by considering the maximum stress value in the section of each finite-element node of wire within a cable portion of length 10 mm in the middle of the bent area. The core wire, whose material properties are different from helical wires, is treated separately.

One observes that infiltrated matrix is responsible for a widening of the stress distribution of layers 2 and 3, whereas layer 1 (core wire) is not affected. It should be noted that this result is consistent with the absence of tension in layer 1, as observed in figure 15.

The impact of matrix penetration on this distribution has been quantified then. Since the distribution from layer 1 is not affected, **only the distributions associated to layers 2 and 3 were analyzed**. For a given distribution **one may consider** the top decile T_{10} , which is the stress value which is only reached or exceeded by 10% of the elements of the distribution. This quantity is interesting since it provides information about the higher stresses, which are likely to initiate damage. The ratio T_{10}^B/T_{10}^A of the deciles from distributions



(a) Layer 1



(b) Layers 2 and 3

Figure 17: Distribution of the maximum stress in wire sections - $R = 10$ mm - Comparison of infiltrated composite B1 (high stiffness's K evaluated in section 3) to non infiltrated composite.

of composites A and B is eventually computed to quantify the increase of the higher stresses of the distribution.

Figure 18 plots the evolution of this ratio as a function of the radius R of bent specimens. Computations have been made using composite B1 from the one hand, and composite B2 on the other one. When considering composite B1, it is observed that the increase of the higher stresses can reach until 7%, even though the plotted ratio decreases for high curvatures. When considering composite B2, the extreme values of the distribution are far less

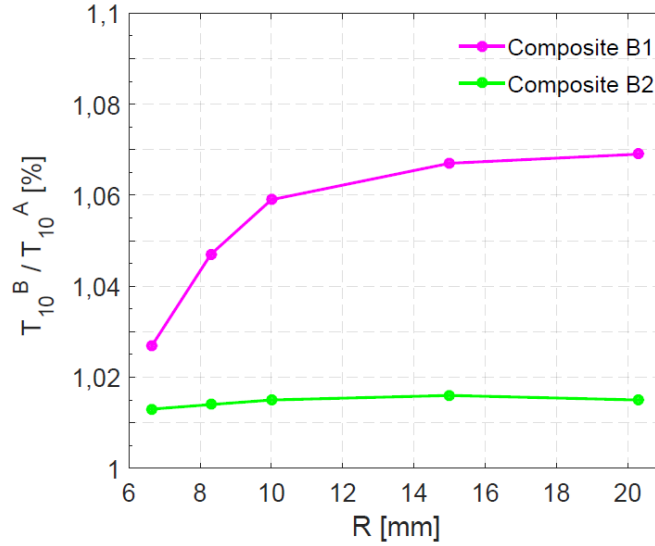


Figure 18: Quantification of the increase of stress due to the presence of infiltrated matrix in composites B1 (high stiffness's K evaluated in section 3) and B2 (stiffness's K representative of the real composite)

impacted by matrix penetration: the increase of the higher stresses doesn't exceed 2% and barely depends on the radius R .

Thus, when considering the infiltrated composite from this study, matrix penetration doesn't have much influence on the higher stresses in wires. It is responsible for a non negligible increase of bending stiffness though, reflected by an increase of 18% of the measured force on the bending device.

Besides, comparisons between composites B1 and B2 points out that increasing rubber stiffness is responsible for an increase of the higher stresses in wires. Depending on rubber properties, matrix penetration could have a detrimental effect on fatigue properties of composite specimens subjected to a bending loading.

5.2. Limitations of infiltrated matrix modelling

As already mentioned, both methods proposed in 3 to evaluate the stiffness's of junction elements lead to overestimated values. The following discusses the possible reasons for these differences.

It has been observed in 3 that the bending of a composite leads to significant inter-wire motions that can reach until $50\ \mu\text{m}$. For such cases, the thinner areas in infiltrated matrix are subjected to very high shear strains, which might induce damage at a microscopic scale. Such phenomena are likely to modify the mechanical properties of rubber, which is not accounted in the models proposed to evaluate the stiffness's K . Thus, the present overestimation of stiffness's might be explained by the non consideration of a change of the local mechanical properties of rubber in the thinner parts of infiltrated areas.

The difference could also be attributed to the manufacturing process, which could imply a different mechanical behavior of the infiltrated matrix compared to bulk matrix (presence of non penetrated areas, uncontrolled pressure conditions during rubber vulcanization, etc...).

Nevertheless, it should be highlighted that the values of K/L_0 predicted by the methods presented in 3 are of the same order of magnitude as the one used to fit experimental data. This gives credence to the interpretation proposed in this work about the influence of infiltrated matrix.

6. Conclusions

The results of this work can be summarized as follows:

1. A finite-element model coupling a cable beam model with a 3D mesh of rubber matrix around the cable has been presented, tested and validated against experimental measurements.
2. An experimental device has been specifically developed to bend composite specimens. An accurate measure of the reaction force applied to specimens for severe bending was carried out. Experimental measurements revealed that composites fully infiltrated by matrix have a higher bending stiffness than non infiltrated ones.
3. A validation procedure was developed, based on the measure of the reaction force on the experimental device. In particular, the error associated to the contribution of rubber to the force in the composite model was found to be negligible, which made it possible to validate directly the cable response of non infiltrated composite.
4. It was proposed to account for infiltrated matrix in composite model by coupling the relative displacements of neighbor wires, assuming that wire-matrix interactions limit inter-wire motions. The coupling was parameterized with stiffness's depending on the thickness of matrix between wires. Two methods based on the analysis of the shearing of the matrix between wires were proposed to evaluate these stiffness's, and lead to similar values.
5. Simulations of fully infiltrated specimen exhibited global responses higher than experimental measurements. This overestimation could be attributed to a possible change of the mechanical properties of the

rubber subjected to large strains in the thinner areas, which is not accounted in the model. A good agreement with the experimental curve was eventually obtained by adjusting stiffness's values.

6. The impact of infiltrated matrix was analyzed. Local interactions between neighbor wires induce tensions in wires, resulting in a shift of the neutral axis of wires. As a result, the higher stresses at the surface of wires increase.

As a final remark, it is worth noting that even if the approach presented in this work has been developed using only one cable architecture, it could also be applied to other cable geometries to study the impact of matrix penetration.

Acknowledgments

This work benefited from the support of the French tyre manufacturer MICHELIN.

References

- [1] W. Jiang, M. Warby, J. Henshall, *Statically indeterminate contacts in axially loaded wire strand*, European Journal of Mechanics and Solids 27 (2008) 69–78.
- [2] R. Judge, Z. Yang, S. Jones, G. Beattie, *Full 3D finite element modelling of spiral strand cables*, Construction and Building Materials 35 (2012) 452–459.

- [3] D. Wang, D. Zhang, S. Wang, S. Ge, *Finite element analysis of hoisting rope and fretting wear evolution and fatigue life estimation of steel wires*, Engineering Failure Analysis 27 (2013) 173–193.
- [4] S. Kmet, E. Stanova, G. Fedorko, M. Fabian, J. Brodniansky, *Experimental investigation and finite element analysis of a four-layered spiral strand bent over a curved support*, Engineering Structures 57 (2013) 475–483.
- [5] A. Nawrocki, M. Labrosse, *A finite element model for simple straight wire rope strands*, Computers & Structures 77 (4) (2000) 345–359.
- [6] W. Jiang, *A concise finite element model for pure bending analysis of simple wire strand*, International Journal of Mechanical Sciences 54 (2011) 69–73.
- [7] D. Zhang, M. Ostojca-Starzewski, *Finite element solutions to the bending stiffness of a single-layered helically wound cable with internal friction*, Journal of Applied Mechanics 83 (3) (2016) 031003.
- [8] W. Jiang, M. Yao, J. Walton, *A concise finite element model for simple straight wire rope strand*, International Journal of Mechanical Sciences 41 (1999) 143–161.
- [9] C. Erdonmez, C. Imrak, *A finite element model for independent wire rope core with double helical geometry subjected to axial loads*, Sadhana 36 (6) (2011) 995–1008.
- [10] G. Costello, *Theory of Wire Rope*, 2nd Edition, Springer, New-York, 1997.

- [11] W. S. Utting, N. Jones, The response of wire rope strands to axial tensile loads—Part I. Experimental results and theoretical predictions, *International journal of mechanical sciences* 29 (9) (1987) 605–619.
- [12] R. J. Cembrola, T. J. Dudek, Cord/Rubber Material Properties, *Rubber Chemistry and Technology* 58 (4) (1985) 830–856.
- [13] R. Pidaparti, *Hierarchical bending analysis of cord-rubber composites*, *American Institute of Aeronautics and Astronautics Journal* 33 (12) (1995) 2359–2363.
- [14] T. Nam, *Finite element model and experimental studies on rubber-cord composite*, *Vietnam Journal of Mechanics* 29 (4) (2014) 551–561.
- [15] D. Durville, *Contact-friction modeling within elastic beam assemblies: an application to knot tightening*, *Computational Mechanics* 49 (6) (2012) 687–707.
- [16] T. Vu, D. Durville, P. Davies, Finite element simulation of the mechanical behavior of synthetic braided ropes and validation on a tensile test, *International Journal of Solids and Structures* 58 (2015) 106–116.
- [17] D. Durville, I. Baydoun, H. Moustacas, G. Perie, Y. Wielhorski, Determining the initial configuration and characterizing the mechanical properties of 3d angle-interlock fabrics using finite element simulation, *International Journal of Solids and Structures* (2018, (in press)) .
- [18] P. J. Armstrong, C. O. Frederick, A mathematical representation of the multiaxial Bauschinger effect, *Tech. Rep. Central Electricity Generating*

Board Report RD/B/N731, Berkeley Nuclear Laboratories, Research & Development Dept. (1966).

- [19] R. Marlow, A general first-invariant hyperelastic constitutive model, in: Constitutive Models for rubber III, 2003, pp. 157–160.
- [20] A. Ali, M. Hosseini, B. Sahari, A review of constitutive models for rubber-like materials, American Journal of Engineering and Applied Sciences 3 (1) (2010) 232–239.

1.5